Available online at www.sciencedirect.com
SCIENCE DIRECT®
Pergamon
Cement and Concrete Research 34 (2004) 507–519
CEMENT AND CONCRETE RESEARCH

Fracture characteristics of concrete at early ages

Jin-Keun Kim[a,*], Yun Lee[a], Seong-Tae Yi[b]

[a]Department of Civil and Environmental Engineering, Korea Advanced Institute of Science and Technology (KAIST), Construction Technology Laboratory, Yusong-gu, Taejon, 305-701, South Korea

[b]Department of Civil Engineering, Chung Cheong University, 330, Wolgok-ri, Kangnae-myun, Cheongwon-kun, Chungbuk-do, 363-792, South Korea

Received 18 February 2001; accepted 5 September 2003

Abstract

The purpose of this study is to experimentally investigate, at early ages, the fracture characteristics of concrete such as critical crack tip opening displacement, critical stress intensity factor, fracture energy, and bilinear softening curve based on the concepts of the effective-elastic crack model and the cohesive crack model.

A wedge-splitting test for Mode I was performed on cubical specimens with an initial notch at the edge. By taking various strengths and ages, load–crack mouth opening displacement (CMOD) curves were obtained and these curves were evaluated by linear elastic fracture mechanics and finite element analysis.

The results from the test and analysis indicate that critical crack tip opening displacement decreases and critical stress intensity factor and fracture energy increase with concrete ages from Day 1 to Day 28. By numerical analysis, four parameters of bilinear softening curves from Day 1 to Day 28 were obtained. In addition, it was observed that the parameters f_t and f_1 increase and the parameters w_1 and w_c decrease with increasing age. The obtained fracture parameters and bilinear softening curves at early ages may be used as a fracture criterion and an input data for finite element analysis of concrete at early ages.

Keywords: Fracture characteristics; Wedge-splitting test; Early ages; Concrete

1. Introduction

Most cracks in concrete members occur due to thermal stress, autogenous shrinkage, drying shrinkage, and external causes. In actual construction, structures can collapse by cracks occurring at early ages before complete hardening of the concrete. Specifically, it influences durability and service life of concrete structures. Therefore, the evaluation and control of cracks at early ages are essential.

To evaluate this problem, experimental studies on various crack occurrence factors and a systematic crack analysis are required. Especially, it is important to clarify the fracture characteristics of concrete at early ages.

Presently, representative models suggested for failure of concrete can be categorized into two types. One is effective-elastic crack model, which applies linear elastic fracture mechanics (LEFM) for brittle material, and the other is cohesive crack model, which simulates fracture progression based on softening phenomena occurring only in quasi-brittle materials such as concrete, rock, ice, ceramic, and composite materials.

The purpose of this study is to investigate the material fracture parameters, based on these two models at early ages, such as critical crack tip opening displacement ($CTOD_c$), critical stress intensity factor (K_{Ic}), fracture energy (G_F), and bilinear softening curve, which are considered as fracture characteristics of concrete. These characteristics are evaluated for concrete from an early age to 28 days.

2. Test specimens and test results

2.1. Mixture proportioning

The concrete mixture proportions selected for the wedge-splitting test (WST) and 28-day compressive strength cylinder specimens are listed in Table 1. Type I Portland cement was used. Maximum aggregate size d_a was 19 mm

* Corresponding author. Tel.: +82-42-869-3614; fax: +82-42-869-3610.

E-mail address: kimjinkeun@cais.kaist.ac.kr (J.-K. Kim).

0008-8846/$ – see front matter © 2004 Elsevier Ltd. All rights reserved.
doi:10.1016/j.cemconres.2003.09.011

Table 1
Concrete mixture proportions

w/c (%)	s/a (%)	Unit weight (kg/m^3)				
		W	C	S	G *	SP (%) * *
70	42	185	268	726	1002	0.15
55	42	185	342	727	1030	0.30
30	41	160	533	712	1090	1.00

* Maximum aggregate size of 19 mm.
** Superplasticizer (high-range water-reducing admixture), ratio of cement weight.

and a high-range water-reducing admixture and vibrator were used to improve the workability and consolidation of the concrete.

2.2. Details of test specimens

The dimensions and shape of WST specimens used in the experiments are shown in Fig. 1. An initial crack was made by inserting a steel plate (1 mm in this study) inside the specimen during the casting and then removing the plate after 1 day. A groove was made in the upper part of specimen to place two load devices with roller bearing and to attach the displacement gages (i.e., CMOD clip gage).

All WST specimens and test cylinders were removed from the mold after 24 h and were wet-cured in a curing room with 100% relative humidity (RH) at 23 ± 2 °C until the testing date.

In this study, a single specimen size was adopted due to the limitation of the testing machine. However, many experimental and theoretical investigations show the fracture toughness dependency to specimen size variation. Bazant and Li [1] suggested a procedure to evaluate the effect of size differences for one type of concrete and single-size fracture specimens. Currently, however, there is no definite method and further studies are necessary. In a follow-up study, size effect on fracture characteristics of concrete at early ages will be reported.

2.3. Test procedure

In this study, the wedge-splitting specimen, initially proposed by Linsbauer and Tschegg [2] and later modified by Brühwiler and Wittmann [3] was used. The principle of the WST is schematically represented in Fig. 2. The specimen is placed on a line support fixed to the lower plate of the testing machine (Fig. 2a). Two massive steel loading devices equipped with roller bearings on each side are placed on the top of the specimen (Fig. 2b). A steel profile with two identical wedges is fixed at the upper plate of the testing machine. The actuator of the testing machine is moved so that the wedge enters between the bearings, which results in a horizontal splitting force component (Fig. 2c). Laboratory test setup and test specimen is shown in Fig. 3. From a testing standpoint, the cracking process can be controlled and monitored using the crack mouth opening displacement (CMOD) shown in Fig. 4 [4]. Some notations are also illustrated in this figure.

The fracture section of the specimen is essentially subjected to a bending moment. The vertical load does not affect the crack propagation. The load in the vertical direction and the crack opening displacement (COD) at two points along the crack surface and the location of roller axis are monitored during testing. The rate of loading was controlled by a constant rate (0.002 mm/s) of increment of COD at the location of roller axis. The specimen was monotonically loaded up to the peak load.

2.4. Test results

The specimens for low-, normal-, and high-strength concrete are assigned with LS, NS, and HS as the specimen names, respectively. Concrete compressive strength f_c', splitting tensile strength f_{ct}, and compressive elastic modulus E_c were determined based on an averaged result of three identical ϕ 100 × 200 mm cylinders. Table 2 tabulates the experimental data of f_c', f_{ct}, and E_c of the concrete cylinders where concrete from the same batch was used to cast the WST specimens.

Fig. 5 contains the plots of the averaged value of horizontal load components versus CMOD for the two WST results for LS, NS, and HS, respectively. Fig. 6 shows the average value of CODs, which were obtained at three points located on the constant distance from the initial crack tip, at the peak load. The test results in Fig. 5 show that the load increases as the CMOD increases; however, the value rapidly decreases after a certain point. Point corresponding to the maximum load in Fig. 5 was considered as the critical point, which can be the beginning point of unstable crack progression.

The stages of opening (Mode I) crack growth for a notched specimen shown in Fig. 4 are related to the load–displacement curve shown. In this curve, stable crack growth begins to propagate as the applied load or displacement increases up to the point. Even though the applied load remains constant or decreases, if the load control

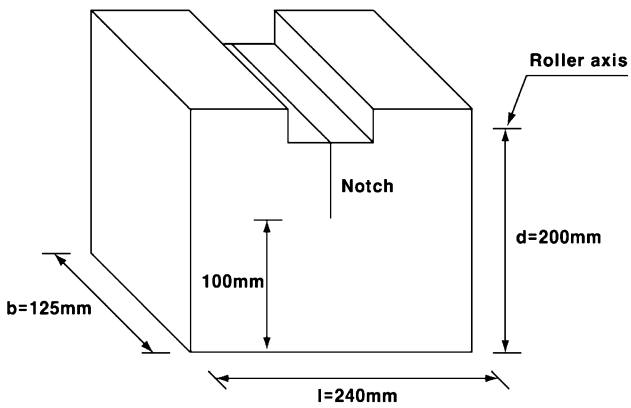

Fig. 1. Geometry and size of specimen.

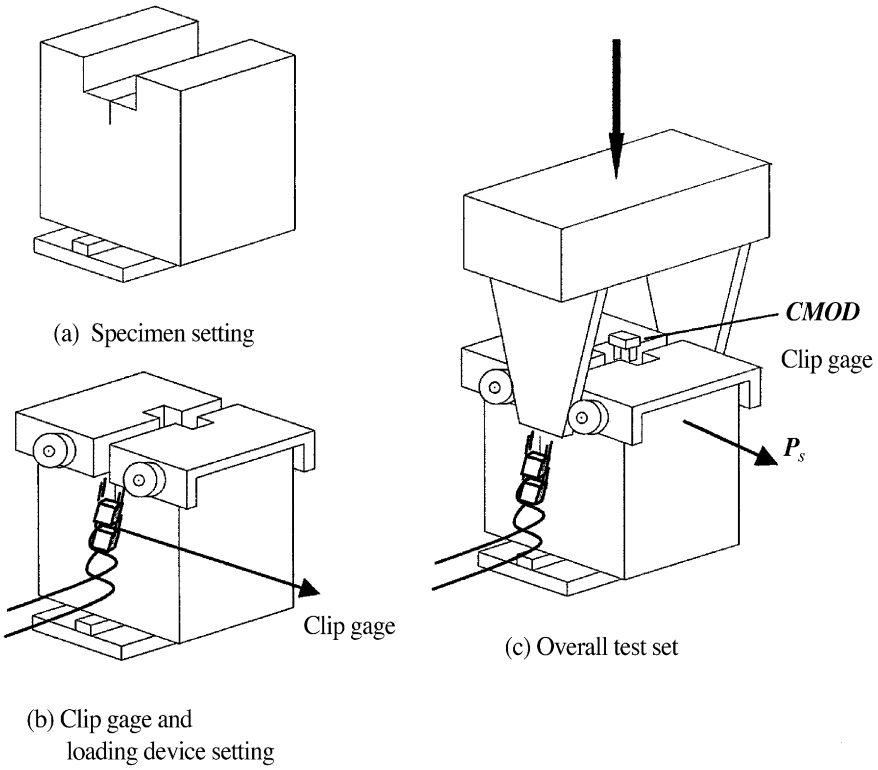

Fig. 2. Principle of WST.

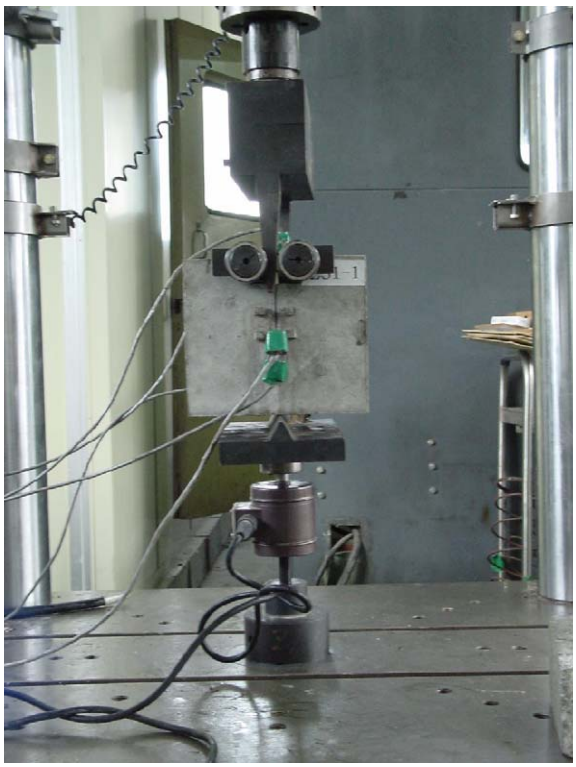

Fig. 3. Laboratory test setup and test specimen.

method is used, the crack propagation can be unstable beyond this point [5]. In this study, however, the displacement control method was used. Accordingly, the testing machine had a way to control it and unstable crack progression did not occur.

Fig. 6 shows that the values measured at three points have a linear relationship. This is related to crack opening profile (shape) (COP), which is discussed in detail in the next section. In this figure, the range of COD values with age is reduced as the strength increases. Fig. 5, load–CMOD curves, is used to obtain the value G_F and the bilinear softening curves. In addition, COD at the peak load (Fig. 6) is used to obtain the values $CTOD_c$ and K_{Ic}.

3. Analysis and evaluation

3.1. Analysis method

To obtain the values $CTOD_c$ and K_{Ic}, which are fracture characteristics based on the effective-elastic crack model, the effective-elastic critical crack length a_{ec} should be determined first. The values $CTOD_c$ and K_{Ic} are fracture parameters used to describe fracture response at the peak load. According to the two-parameter fracture model by Jenq and Shah [6], to obtain the value a_{ec}, which causes elastic fracture response of structures, the test is performed

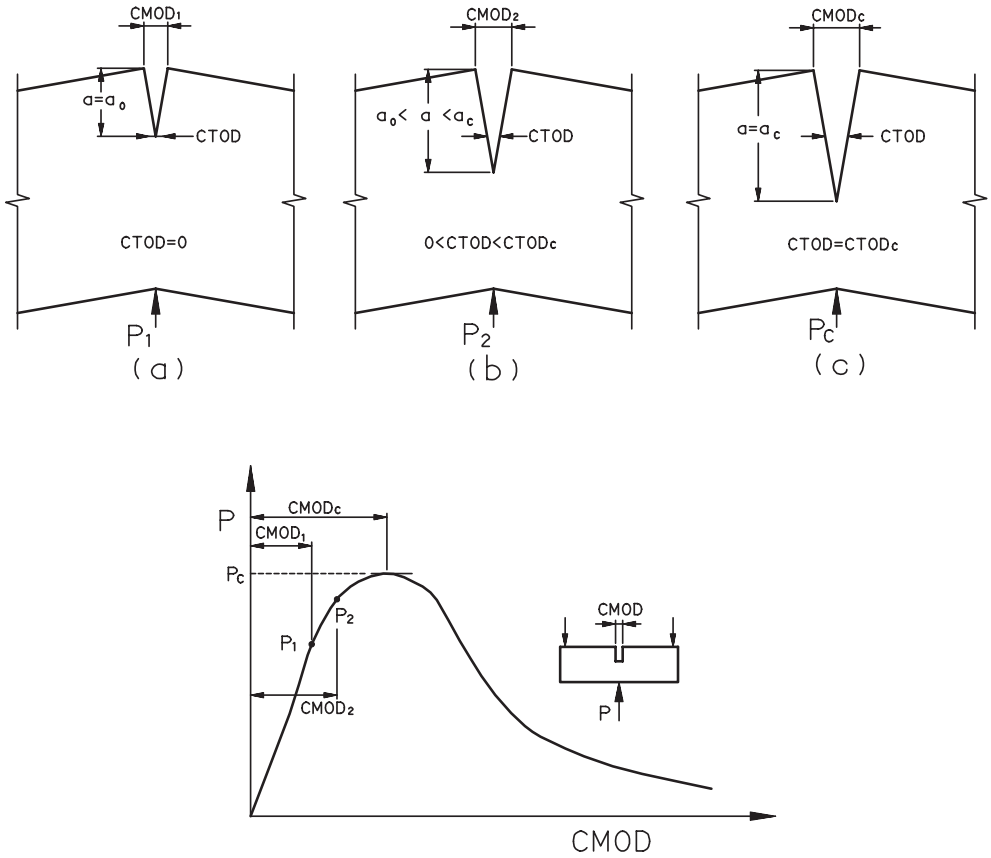

Fig. 4. Stages of Mode I crack growth: (a) initiation of stable crack growth, (b) process zone partially developed, and (c) start of unstable crack growth at peak load [4].

by loading the specimen under CMOD control up to the point beyond the maximum load and then it is unloaded and reloaded.

In Jenq and Shah's model, the value a_{ec} may be defined in such a way that it results in an unloading compliance C_u within 95% of the peak load based on LEFM. However, it is difficult to select the beginning point of unloading and to calculate the value C_u from the load–CMOD curve. Accordingly, in this study, the COP based on LEFM, rather than the unloading compliance, is used to determine the value a_{ec}. This may be expressed as

$$\mathrm{COD}(a,x) = \mathrm{CMOD} \times g\left(\frac{a}{d},\frac{x}{a}\right) \tag{1}$$

$$g\left(\frac{a}{d},\frac{x}{a}\right) = \left\{\left(1-\frac{x}{a}\right)^2 + \left(0.94 - 1.11\frac{a}{d}\right)\left[\frac{x}{a} - \left(\frac{x}{a}\right)^2\right]\right\}^{1/2}$$

where g is the COP function obtained from the finite element (FE) analysis for the WST specimens; a is the crack length; d is the characteristic dimension of a member (in this study, d is regarded as the length from bottom face of a specimen to roller axis); and x is the distance from the roller axis. Namely, Eq. (1) represents the value COD with x as the function of CMOD. The g function curves for different crack lengths are shown in Fig. 7. Fig. 7 shows that the shape of curves around the crack tip is nonlinear, and as it becomes more distant from the crack tip it shows a linear relationship. This is consistent with experimental results. Namely, the values of COD, which was measured at three points (i.e. roller axis, x_1, and x_2 spaced from the crack tip), show nearly a linear relationship.

Table 2
Physical properties of concrete

Type	Age (days)	f_c' (MPa)	f_{ct} (MPa)	E_c (MPa)
LS	1	3.92	0.28	7649
	3	10.30	1.54	19,515
	7	13.73	1.80	21,673
	14	15.59	2.43	23,046
	28	18.53	2.90	26,772
NS	1.5	5.49	1.56	12,945
	3.5	16.48	2.23	22,948
	7.75	22.36	3.27	26,184
	14.75	26.58	3.70	26,870
	28.5	33.24	3.92	28,832
HS	1	16.57	2.90	24,320
	3.25	26.18	3.85	31,283
	7.33	37.27	3.91	32,460
	14.75	52.07	4.59	33,833
	28	57.96	4.86	35,794

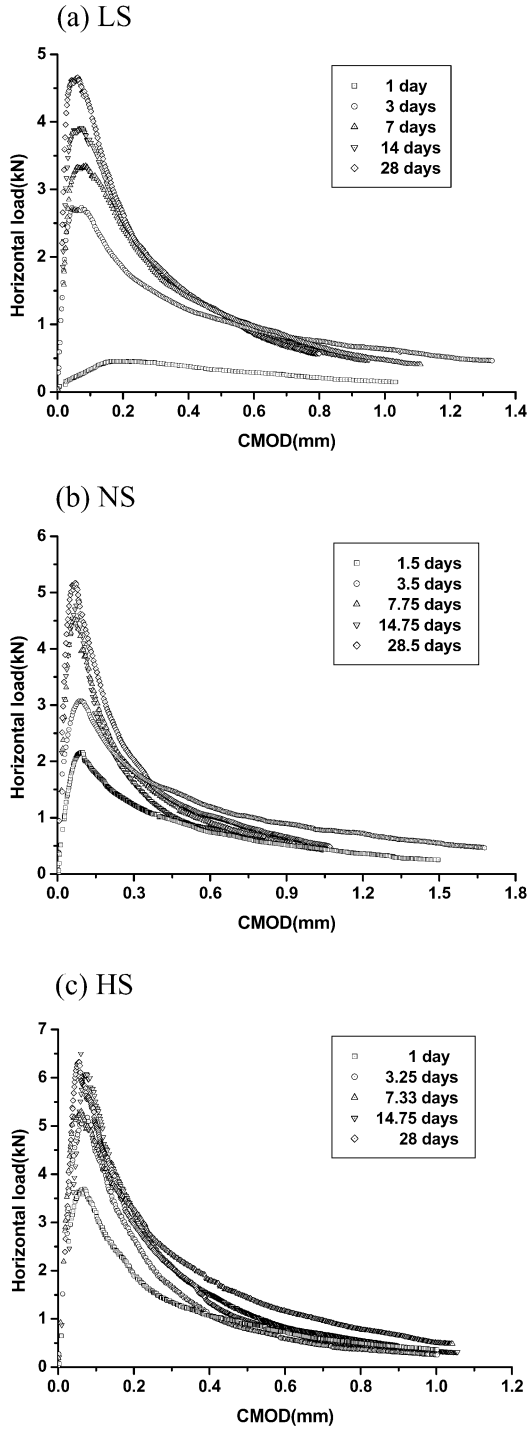

Fig. 5. Horizontal load–CMOD curves.

Two equations for the value a_{ec} can be obtained by substituting two COD(x) values measured at x_1 and x_2 into Eq. (1). Then, by solving Eq. (1), two values for a_{ec} can be determined and, finally, we can obtain the value a_{ec} by averaging these values. After the value a_{ec} is determined, the value $CTOD_c$ can be obtained. The value $CTOD_c$ is determined by substituting the values of a_{ec}, CMOD, and a_o into Eq. (1), where the values a_o and a_{ec}, respectively, instead of x and a, should be used. Finally, the value a_{ec} as well as the critical (peak) load P_c is further substituted into Eq. (2), which is suggested by Murakami [7] to calculate the value K_{Ic}.

$$K_{Ic} = \frac{P_c}{b\sqrt{d}} F(\alpha) \tag{2}$$

$$F(\alpha) = 29.6\alpha^{0.5} - 185.5\alpha^{1.5} + 665.7\alpha^{2.5} - 1017.0\alpha^{3.5} + 638.9\alpha^{4.5}$$

where $F(\alpha)$ is derived by Zhao et al. [8] for conventional WST specimens (i.e. $l/d = 1.2$) like those of this study; b is

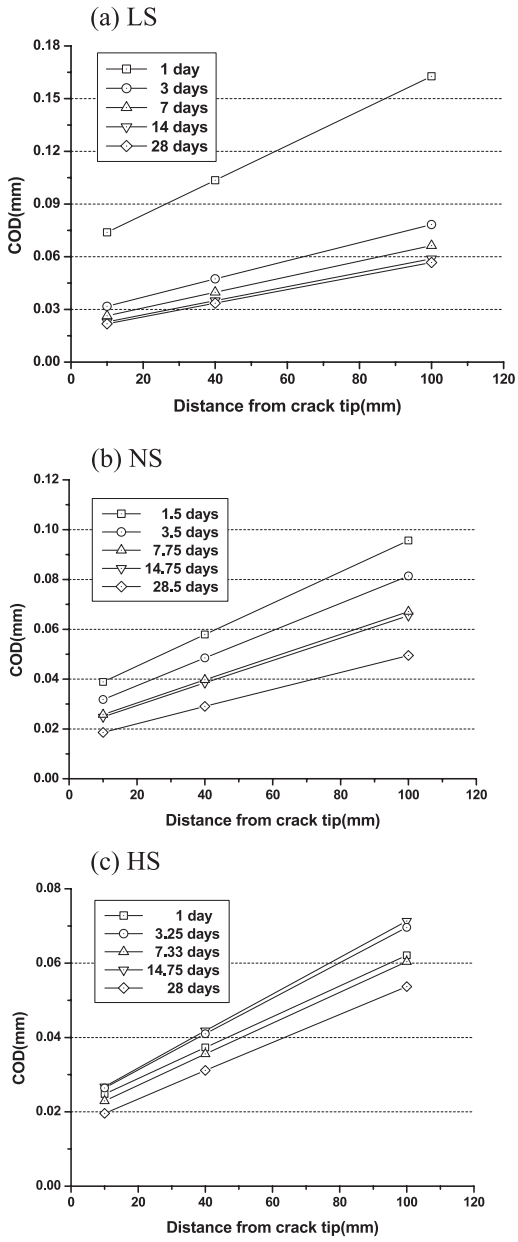

Fig. 6. COD at peak load.

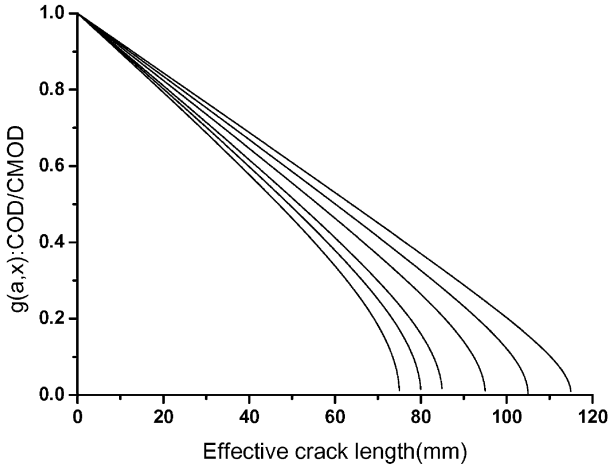

Fig. 7. COP function for WST specimen.

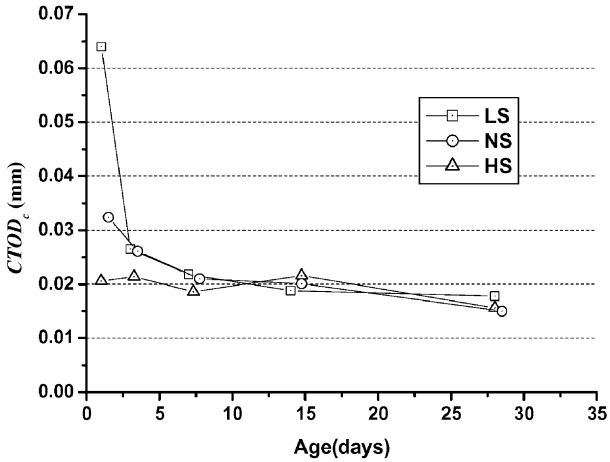

Fig. 9. $CTOD_c$ at various ages.

the thickness of a specimen; l is the length of a specimen; d is the length from bottom face of a specimen to roller axis; $F(\alpha)$ is the constant given by the initial crack length a_o; and α is a/d. Based on the obtained load–CMOD curve of Fig. 5, the fracture energy G_F can be calculated.

3.2. Analysis results

Fracture characteristics obtained from the analyses are graphed and shown in Figs. 8–11 and Table 3. Based on critical effective crack extension Δa_{ec} (where the value Δa_{ec} is given by $a_{ec} - a_o$) indicated in Fig. 8, it is noted that crack propagates more up to the peak load as strength is lower and age is younger. In addition, as predicted in the COD shape of Fig. 7, the value $CTOD_c$ in Fig. 9 also increases with lower strength and younger age. There is a similar pattern with Δa_{ec}. According to Figs. 10 and 11, the values K_{Ic} and G_F increase with increasing age, especially increasing rapidly at early ages, and converging to a limit at 28 days. This means that the fracture toughness increases rapidly with increasing early age after the casting. The values K_{Ic} are compared with the results obtained from three-point bend beam tests at 0.5, 1, 7, 21, and 28 days by Zollinger et al. [9]. Although there is a difference in the results due to the difference of materials and experimental methods used, it seems the trend is similar.

3.3. Bilinear softening curve by numerical analysis

A typical softening curve of concrete is shown in Fig. 12. Petersson [10] proposed a method for equating the softening curve with the bilinear softening curve as shown in Fig. 13. This indicates that the softening curve (i.e., the curve is the one of fracture characteristics of concrete) can be simplified by determining f_t, f_1, w_1, and w_c values. It is noted that the bilinear curve can be completely determined

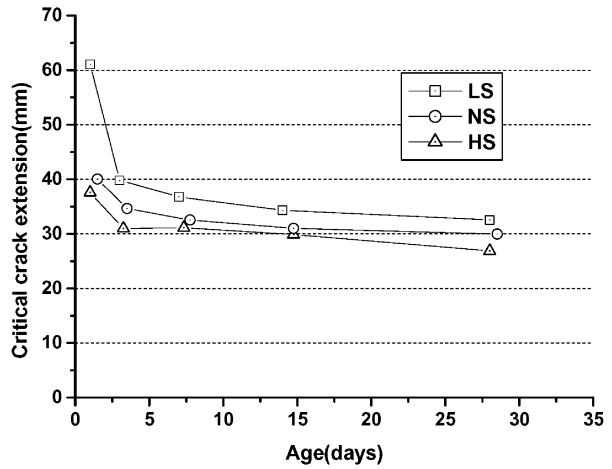

Fig. 8. Critical effective crack extension Δa_{ec} at various ages.

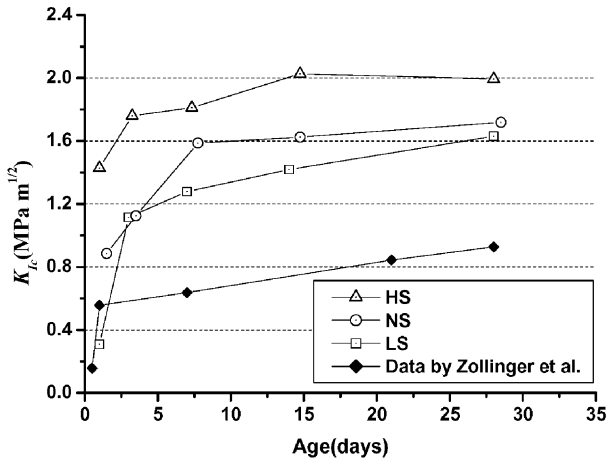

Fig. 10. K_{Ic} at various ages.

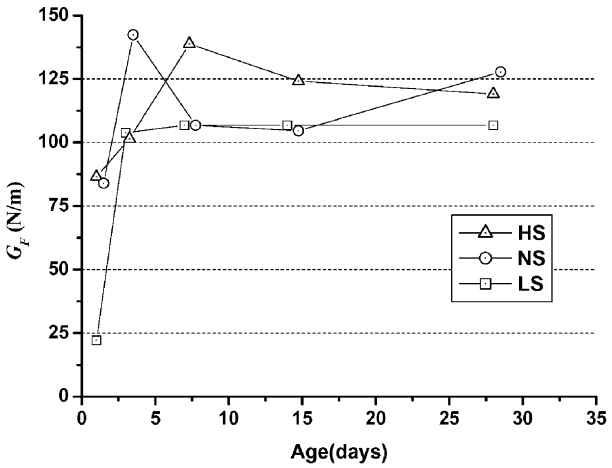

Fig. 11. G_F at various ages.

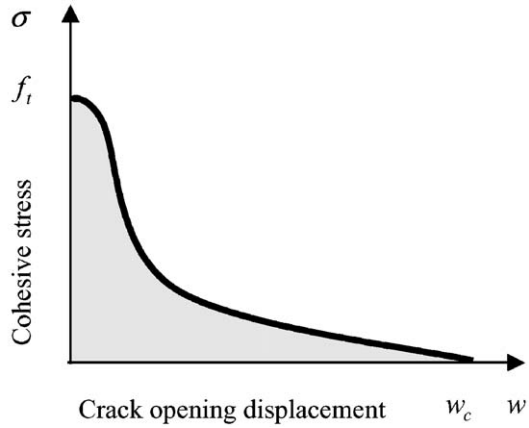

Fig. 12. Softening curve of concrete.

if the f_t, f_1, w_1 and w_c values are known. In this study, FE analysis was carried out based on the cohesive crack model and the principle of superposition suggested by Gopalaratnam and Ye [11] in 1991. First, from crack analysis using superposition we can obtain the independent elastic solution for the external load and a unit load applied at point x along the crack surfaces of fracture process zone (FPZ). Second, to satisfy equilibrium equation, compatibility condition, and cohesive stress–COD relationship in the FPZ for overall structures, a series of equation systems is composed.

In this study, the stress condition was assumed as plane-stress and the specimen configuration and the finite element mesh used for numerical investigation are shown in Fig. 14. As an input data for FE analysis, initial tangent modulus in tension $E_0 \approx 1.5E_c$ was used. This modulus was selected from trial and error method by FE analysis to obtain the closest approximation to load–CMOD curves shown in Fig. 5. Where E_c is the compressive elastic modulus.

Only half of the specimen needs to be considered due to symmetry. There were a total of 390 elements (two-dimensional parabolic isoparametric element) and 23 nodes on the ligament length $d - a_o$ where the crack propagates. At these nodes, the load–COD relationship for FE analysis was obtained using the nonlinear spring element, which shows the bilinear softening phenomena. From the load–CMOD curve, four parameters for bilinear softening curve, f_t, f_1, w_1 and w_c, can be obtained. To obtain the optimum solution for the load–CMOD curve, the following function is used.

$$F(f_t, f_1, w_1, w_c) = \int_0^{\mathrm{CMOD_o}} (P_e - P_m)^2 d\delta \tag{3}$$

where P_e is the load obtained from the tests, $\mathrm{CMOD_o}$ is equal to an ideal value CMOD when the load is 0.0, and $P_m = P_m(f_t, f_1, w_1, w_c)$ is the load obtained from FE

Table 3
Fracture characteristics of concrete at early ages

Type	Age (days)	Δa_{ec} (mm)	$\mathrm{CTOD_c}$ (mm)	K_{Ic} (MPa $m^{1/2}$)	G_F (N/m)
LS	1	61.05	0.0640	0.3088	22.08
	3	39.78	0.0265	1.1151	103.83
	7	36.78	0.0218	1.2783	106.77
	14	34.34	0.0188	1.4185	106.80
	28	32.56	0.0178	1.6299	106.81
NS	1.5	40.04	0.0324	0.8854	83.93
	3.5	34.66	0.0261	1.1241	142.38
	7.75	32.54	0.0210	1.5869	106.80
	14.75	31.02	0.0201	1.6243	104.65
	28.5	29.96	0.0150	1.7178	127.74
HS	1	37.56	0.0206	1.4282	86.44
	3.25	30.99	0.0214	1.7593	101.49
	7.33	31.11	0.0186	1.8114	138.84
	14.75	29.88	0.0216	2.0267	124.08
	28	26.87	0.0156	1.9941	119.04

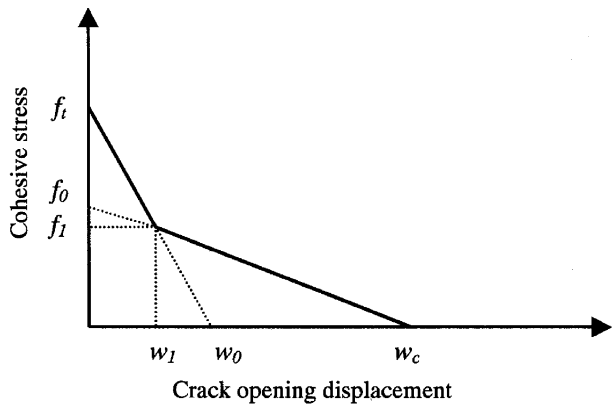

Fig. 13. Bilinear softening curve.

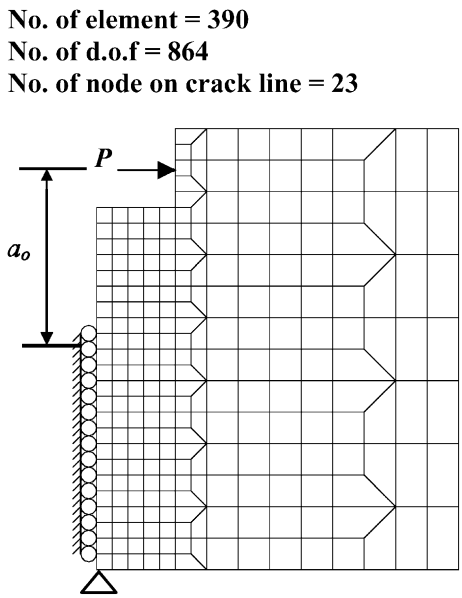

Fig. 14. Specimen configuration and FE mesh.

analysis. The function $F(f_t, f_1, w_1, w_c)$ represents the difference between the load–CMOD curve obtained from the tests and the load–CMOD curve obtained from the analysis. Therefore, the softening curve can be said to be more accurate when $F(f_t, f_1, w_1, w_c)$ has a minimal value. The condition is shown in Eq. (4).

$$\frac{\partial F}{\partial f_t} = \frac{\partial F}{\partial f_1} = \frac{\partial F}{\partial w_1} = \frac{\partial F}{\partial w_c} = 0 \tag{4}$$

Eq. (4) shows four nonlinear equations. To solve these equations, the Newton–Raphson iteration method was

Table 4
Parameters of bilinear softening curve obtained by numerical analysis

Type	Age (days)	f_t (MPa)	f_1 (MPa)	w_1 (mm)	w_c (mm)	$F(f_t, f_1, w_1, w_c)$ (kN^2 mm)
LS	1	0.1657	0.1153	0.0334	0.2998	0.0047
	3	1.2955	0.4183	0.0188	0.3338	0.0297
	7	1.4392	0.4159	0.0310	0.3551	0.0270
	14	1.7776	0.4253	0.0284	0.2585	0.0350
	28	2.5579	0.6616	0.0122	0.1672	0.0887
NS	1.5	0.9204	0.2995	0.0269	0.3896	0.0162
	3.5	1.3168	0.4336	0.0304	0.3627	0.0168
	7.75	2.1135	0.4625	0.0224	0.2450	0.0269
	14.75	2.4676	0.4978	0.0154	0.2217	0.0630
	28.5	2.8304	0.6275	0.0133	0.2101	0.1067
HS	1	1.7758	0.4023	0.0181	0.2749	0.0287
	3.25	2.6245	0.5677	0.0156	0.1722	0.1180
	7.33	2.6315	0.6743	0.0166	0.1822	0.1444
	14.75	3.0572	0.6865	0.0159	0.1746	0.1877
	28	3.3044	0.6638	0.0149	0.1646	0.1443

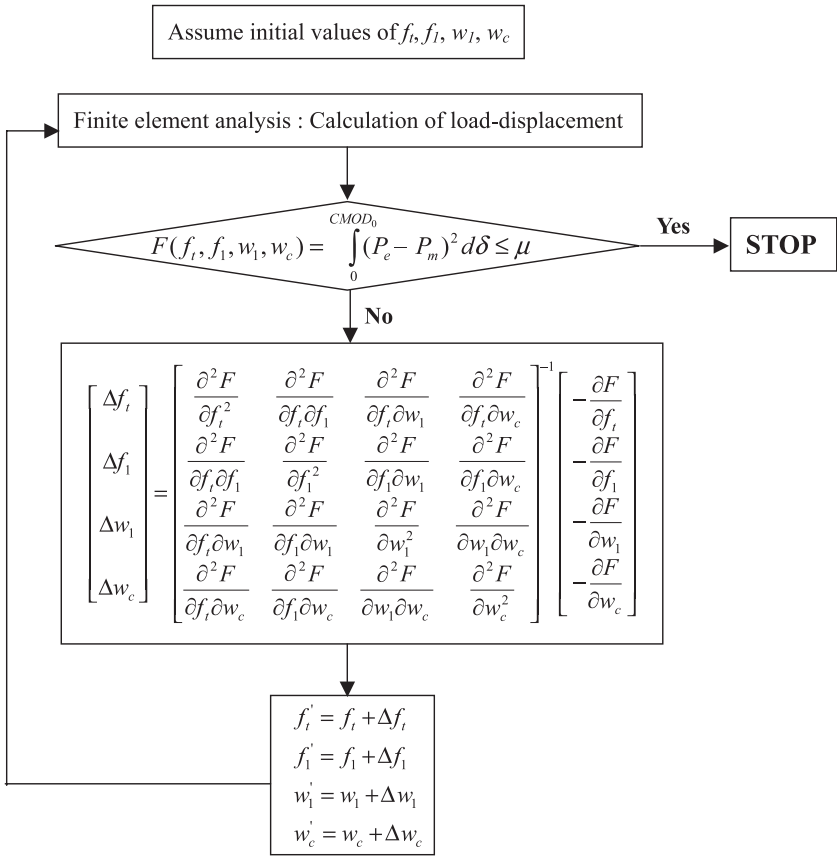

Fig. 15. Flow chart of the numerical procedure.

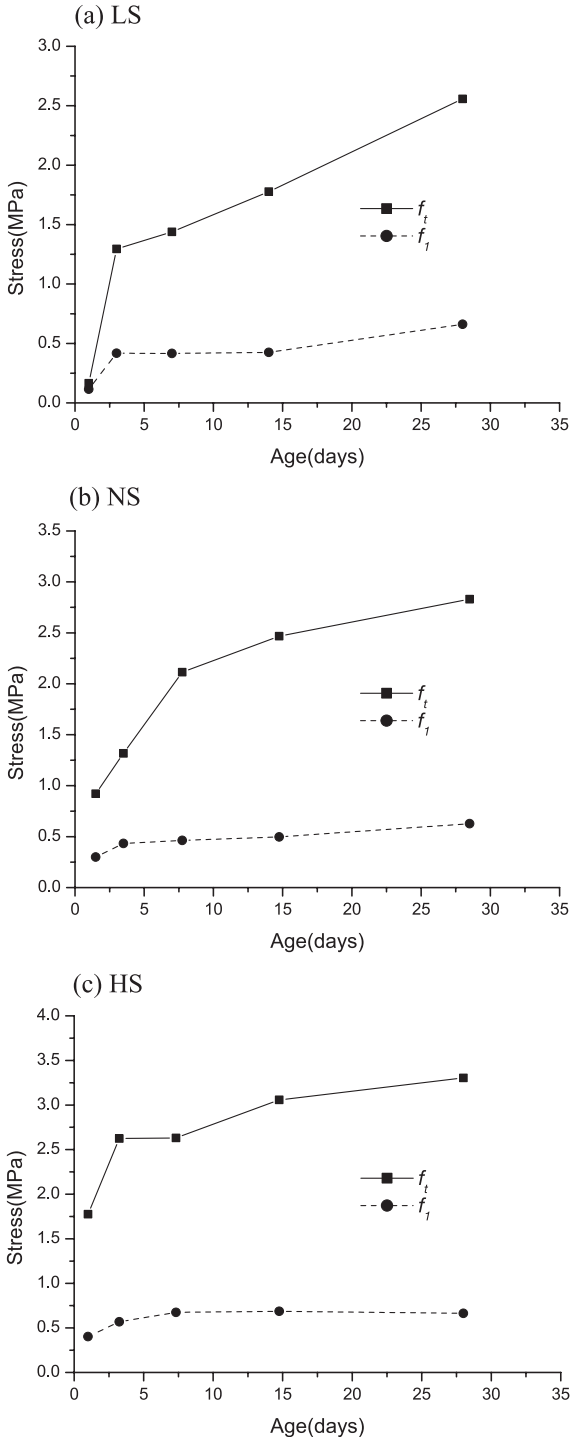

Fig. 16. Variation of parameters f_t and f_1 with age.

used. The procedure is shown in Fig. 15 [12–14]. The differential terms of $F(f_t, f_1, w_1, w_c)$ shown in Fig. 15 can be calculated by numerical method as shown in Eq. (5) [14].

$$\frac{\partial f}{\partial x} \approx \frac{f(x+h) - f(x-h)}{2h} \tag{5}$$

$$\frac{\partial^2 f}{\partial x^2} \approx \frac{f(x+h) + f(x-h) - 2f(x)}{h^2}$$

$$\frac{\partial^2 f}{\partial x \partial y} \approx \frac{f(x+h, y+g) + f(x-h, y-g)}{4hg} - \frac{f(x+h, y-g) + f(x-h, y+g)}{4hg}$$

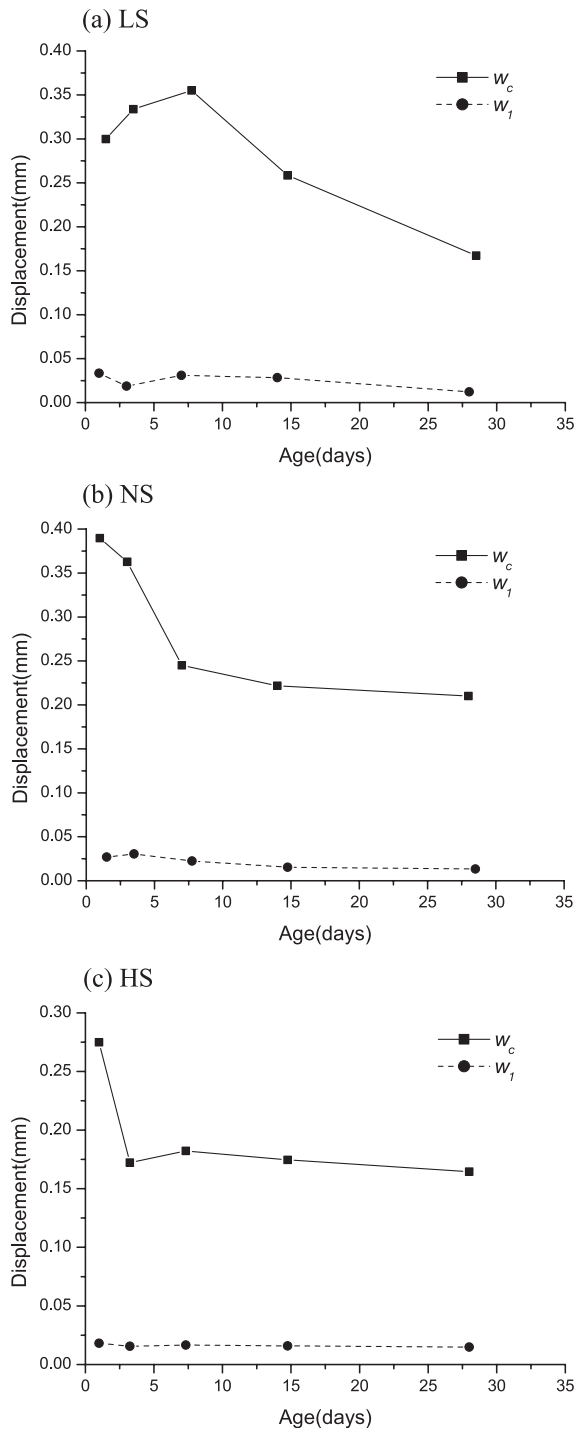

Fig. 17. Variation of parameters w_c and w_1 with age.

where the values g and h are sufficiently small positive constants.

The parameters f_t, f_1, w_1, and w_c for bilinear softening curves obtained from numerical analysis are summarized in Table 4, Fig. 16, and Fig. 17. According to Figs. 16 and 17, the parameters f_t and f_1 increase and the parameters w_1 and w_c decrease as age increases. This is because the peak load and the brittleness of load–CMOD curve with age increases up to the peak load. However, the curve shows more rapid softening phenomena after the peak load with increasing age.

In the ideal case, the minimum value of $F(f_t, f_1, w_1, w_c)$ shall be 0.0. In this study, however, due to experimental and analytical reasons, this value is not 0.0 but is a positive constant. According to Table 4, the averaged values of $F(f_t, f_1, w_1, w_c)$ are 0.0370, 0.0459, and 0.1246 kN^2 mm, respectively, in cases of LS, NS, and HS. However, if we consider that the integral limit ($CMOD_o$) is 2.0 mm, the errors are 0.136, 0.151, and 0.250 kN on each CMOD value of load–CMOD curves, respectively, for LS, NS, and HS cases. The reasons for the increase of these errors as the strength increases are that the peak load increases on the

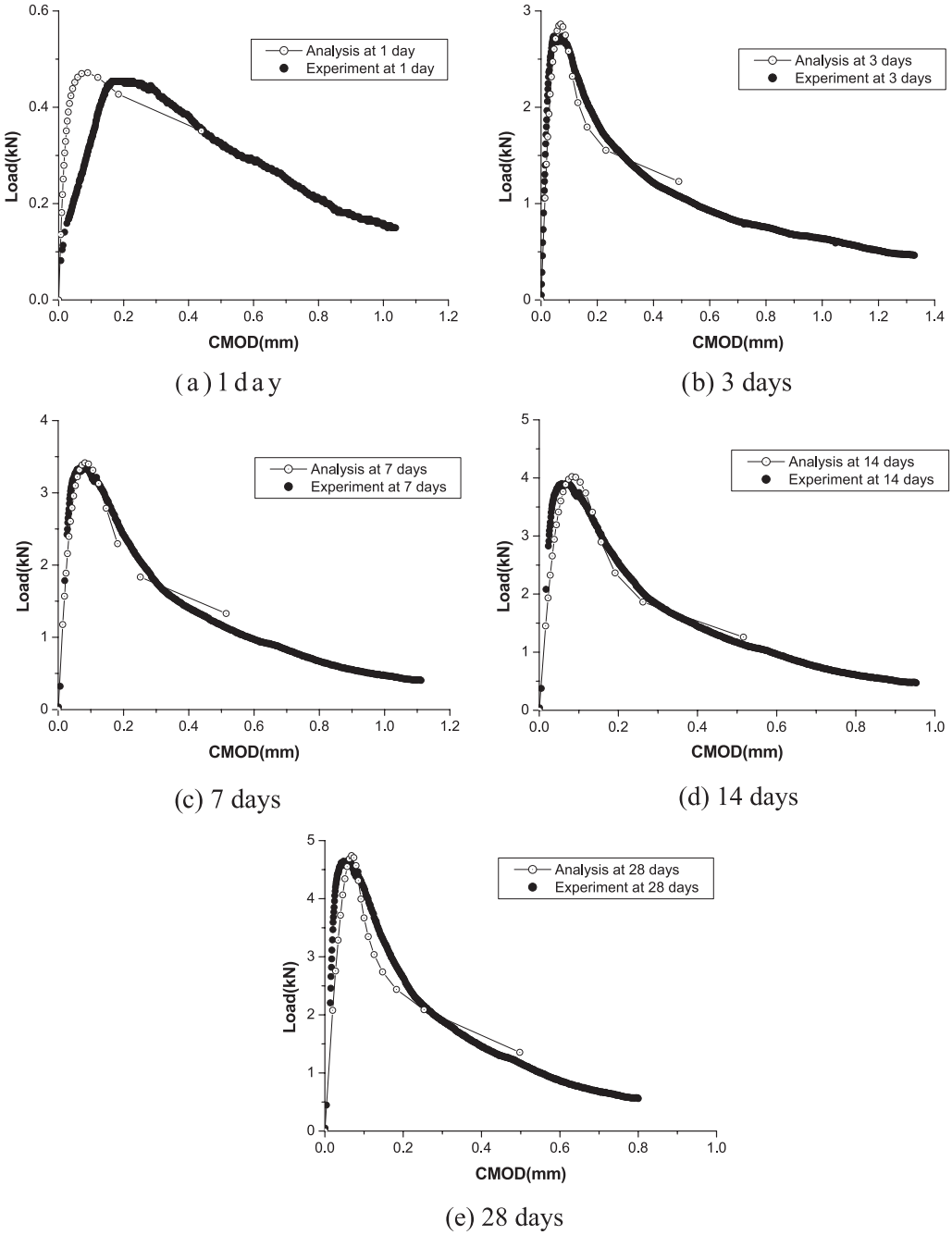

Fig. 18. Load–CMOD curves with age for LS (numerical analysis).

load–CMOD curve and the load reduction happens more rapidly after the peak load as the strength increases. In this study, for three levels of strength, the same number of nodes on the ligament in which the crack propagates is used. Accordingly, the error increases around the load transition point as the strength increases. For HS, to reduce the error, the number of nodes on the ligament should increase.

It is seen in Figs. 18–20 that load–CMOD curves from the analyses using four parameters obtained are comparable with ones from the tests. In Fig. 18(a), however, a considerable difference is evident because the load–CMOD curve at 1 day for LS is severely nonlinear up to the peak load.

4. Conclusions

In this study, fracture characteristics of concrete with age, specifically at early ages, were investigated and the results can be summarized as follow:

1. Instead of performing an unloading cycle on the route of experiments, the value a_{ec}, which the effective-elastic

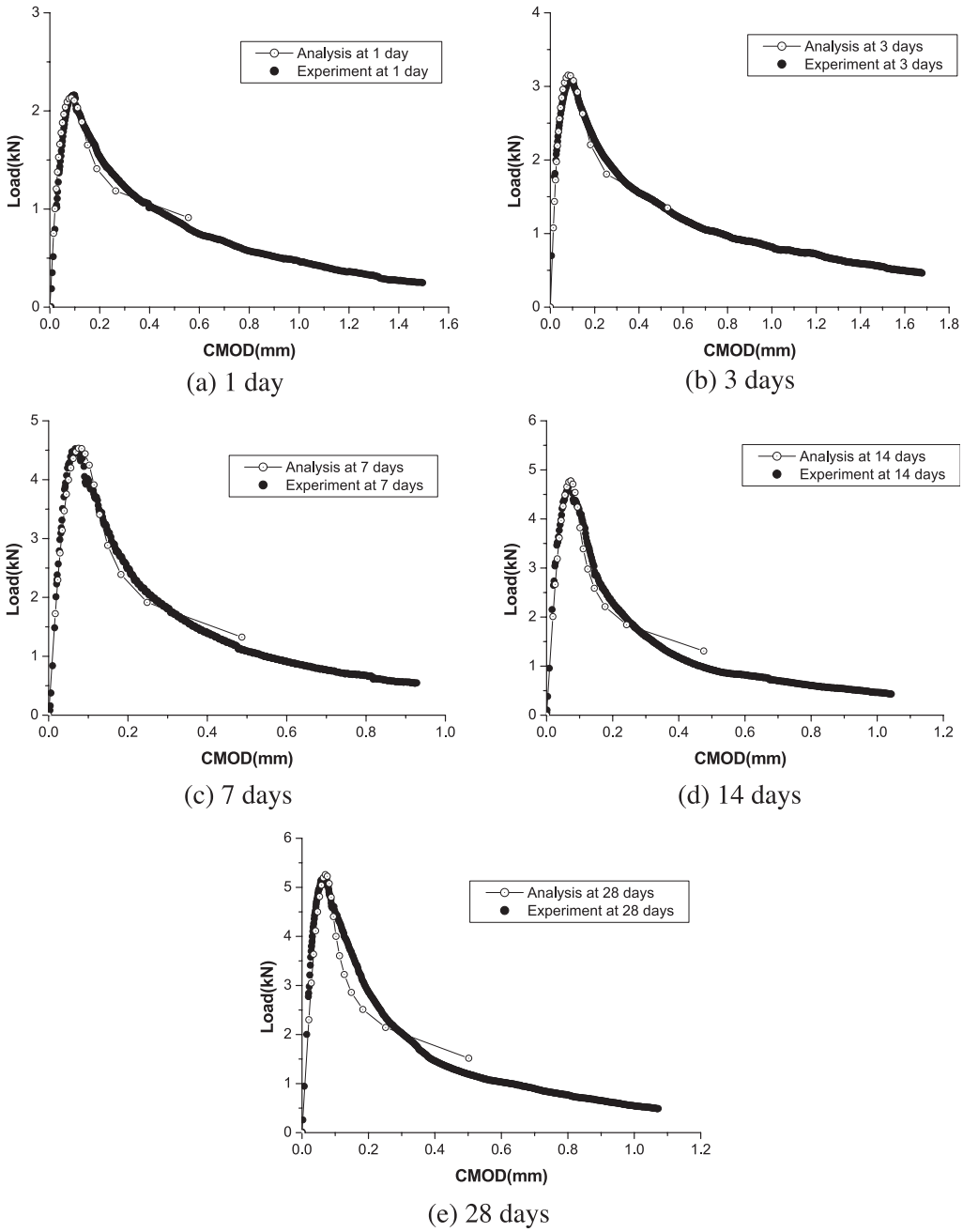

Fig. 19. Load–CMOD curves with age for NS (numerical analysis).

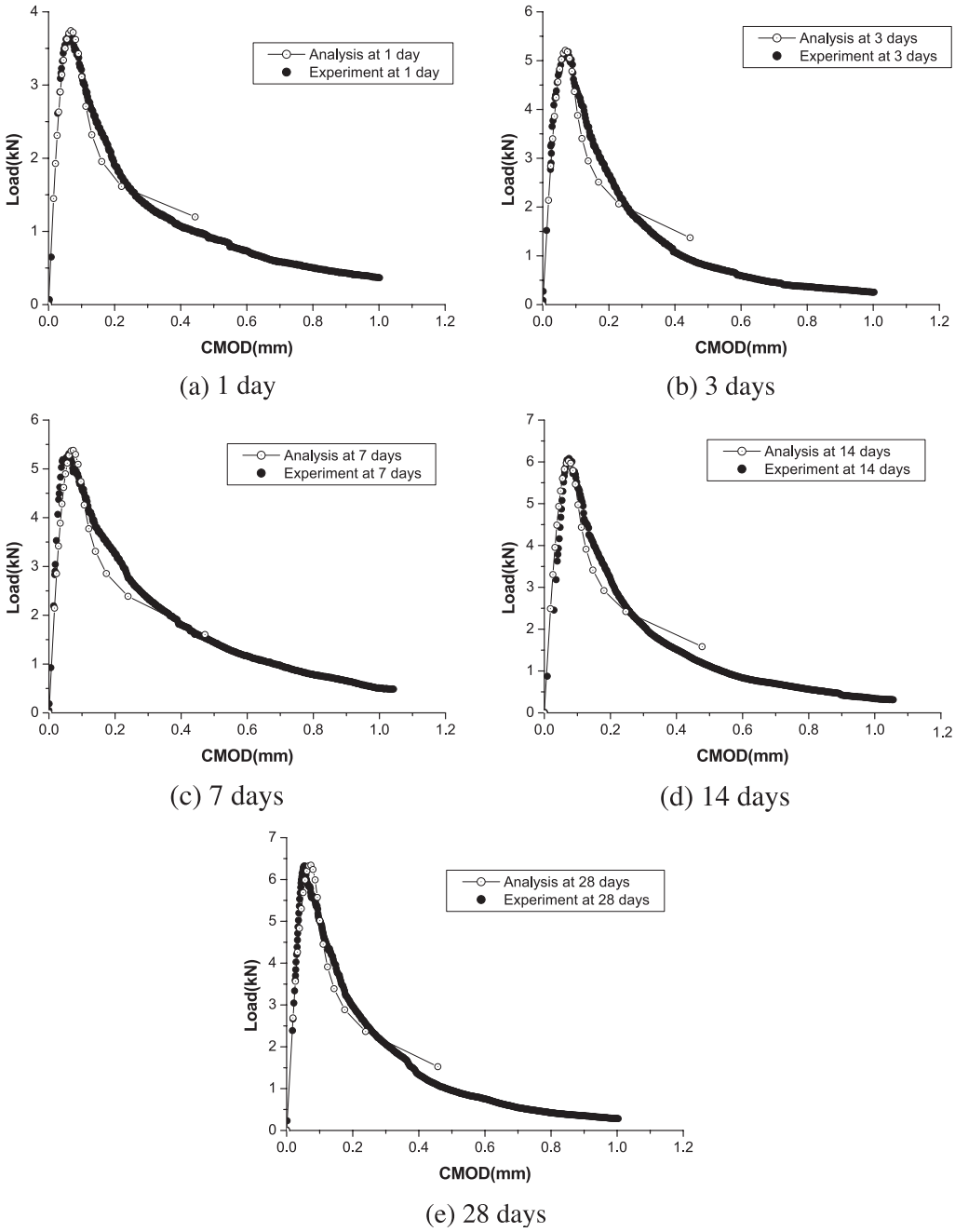

Fig. 20. Load–CMOD curves with age for HS (numerical analysis).

crack model defines, was derived using the results obtained from the stable WST and the COP for WST specimens.

2. Using the value a_{ec}, the values $CTOD_c$ and K_{Ic}, which are fracture characteristics, for concrete at early ages were obtained. The value G_F for concrete at early ages was determined based on the load–CMOD curve obtained from the WST.
3. Based on the cohesive crack model, the bilinear softening curves of concrete at early ages were determined by comparing the load–CMOD curve obtained from FE analysis of specimens used in this study with the load–CMOD curve obtained from the tests.
4. The derived fracture parameters and bilinear softening curves at early ages may be used as a fracture criterion and input data for FE analysis of concrete at early ages.

5. Further experiment

Because this experimental study was conducted for a single specimen size and measurements were performed when the FPZ has not yet attained a steady-state size, further experimental work involving the specimen sizes decreasing and increasing at early ages would be required.

Notation

a	crack length
a_c	critical crack length
a_o	initial crack length
a_{ec}	effective-elastic critical crack length
b	thickness of a specimen
C_u	unloading compliance within 95% of the peak load for load–CMOD curve
COD	crack opening displacement
COP	crack opening profile
CMOD	crack mouth opening displacement
$CMOD_c$	critical crack mouth opening displacement
CTOD	crack tip opening displacement
$CTOD_c$	critical crack tip opening displacement
$CMOD_o$	CMOD value when the load is 0.0
d	length from bottom face of a specimen to roller axis
$d - a_o$	ligament length
d_a	maximum aggregate size
E_c	compressive elastic modulus of concrete
E_o	initial tangent modulus in tension
f_c'	compressive strength of concrete
f_{ct}	splitting tensile strength of concrete cylinder
f_t, f_1, w_1, w_c	four parameters for bilinear softening curve
g	crack opening profile function
G_F	fracture energy
K_{Ic}	critical stress intensity factor
l	length of a specimen
P	applied force
P_c	critical (peak) load
P_e	load obtained from the tests
P_m	load obtained from FE analysis
x, x_1, x_2	distance from the roller axis along the crack surface
Δa_{ec}	critical effective crack extension length

Acknowledgements

The authors would like to thank the Korea Institute of Science and Technology Evaluation and Planning (KISTEP) for the financial support of the National Research Laboratory (NRL).

References

[1] Z.P. Bazant, Z. Li, Zero-brittleness size-effect method for one-size fracture test of concrete, J. Eng. Mech., ASCE 122 (5) (1996) 458–468.
[2] H.N. Linsbauer, E.K. Tschegg, Fracture energy determination of concrete with cube-shaped specimens, Zem. Beton 31 (1986) 38–40.
[3] E. Brühwiler, F.H. Wittmann, The wedge splitting test, a new method of performing stable fracture mechanics tests, Eng. Fract. Mech. 35 (1/2/3) (1990) 117–125.
[4] S.P. Shah, S.E. Swartz, C. Ouyang, Fracture Mechanics of Concrete: Applications of Fracture Mechanics to Concrete, Rock, and Other Quasi-Brittle Materials, Wiley, 1995, 552 pp.
[5] S. Xu, H.W. Reinhardt, Determination of double-k criterion for crack propagation in quasi-brittle fracture: Part III. Compact tension specimens and wedge splitting specimens, Int. J. Fract. 98 (1999) 179–193.
[6] Y.S. Jenq, S.P. Shah, A two parameter fracture model for concrete, J. Eng. Mech., ASCE 111 (4) (1985) 1227–1241.
[7] Y. Murakami, Stress Intensity Factors Handbook, Pergamon, New York, 1987.
[8] G. Zhao, H. Jiao, S. Xu, Study on Fracture Behavior with Wedge Splitting Test Method, Fracture Processes in Concrete, Rock and Ceramics, E & FN Spon, London, 1991, pp. 789–798.
[9] D.G. Zollinger, T. Tang, R.H. Yoo, Fracture toughness of concrete at early ages, ACI Mater. J. 90 (5) (1993) 463–471.
[10] P.E. Petersson, Crack Growth and Development of Fracture Zones in Plain Concrete and Similar Materials, Report No. TVBM-1006, Division of Building Materials, Lund Institute of Technology, Lund, Sweden, 1981.
[11] V.S. Gopalaratnam, B.S. Ye, Numerical characterization of the nonlinear fracture process in concrete, Eng. Fract. Mech. 40 (6).
[12] P.E. Roelfstra, F.H. Wittmann, in: F.H. Wittmann (Ed.), Numerical Method to Link Strain Softening with Failure of Concrete, Fracture Toughness and Fracture Energy of Concrete, Elsevier Science, Amsterdam, 1986, pp. 163–175.
[13] H. Mihashi, N. Nomura, Correlation between characteristics of fracture process zone and tension-softening properties of concrete, Nucl. Eng. Des. 165 (3).
[14] S.H. Eo, J.K. Kim, H.S. Kim, Numerical investigation of fracture characteristics and size effect for high strength concrete beam, J. Korean Soc. Civ. Eng. 17 (I-3) (1997) 361–371 (in Korean).